Journal of the Physical Society of Japan
Vol. 74, No. 2, February, 2005, pp. 568–576

The Molecular Effect in the Multiple Ionization of Diatom Molecules by Fast Ion Impact

Takao WADA and Toshiaki KANEKO

Graduate School of Science, Okayama University of Science, 1-1 Ridai-cho, Okayama 700-0005

(Received July 15, 2004)

The multiple ionization process is investigated for the molecular targets on the basis of the recently developed contracted independent electron model (CIEM), where the impact-parameter-dependent ionization probability plays a key role. We found that the multiple ionization cross sections strongly depend on the angle between the incident beam direction and the molecular axis. Also the molecular effect is found that the ionization cross section for a molecular target is not equal to the sum of those for the constituent isolated atoms. Moreover, we proved the sum rule on the net ionization cross section. Numerical estimation shows that the multiple ionization cross sections for N_2 and CO molecules, bombarded by the ions at the energies of more than 100 keV/u, are in better agreement with the experimental data than the other models.

KEYWORDS: collision, multiple ionization, molecular effect
DOI: 10.1143/JPSJ.74.568

1. Introduction

The electron excitation and the related processes have been intensively studied as a basic knowledge in the fields of atomic collisions in solids, plasma-wall interaction, energy deposition in materials, and environmental physics. Among them, a great interest in the multiple ionization process has been taken for the molecular- and the cluster-targets by the fast ion impact. The motivation of this study is to know (1) the cross sections as a function of the incident velocity,[1–5] (2) the correlation with the incident beam direction,[6–12] (3) the charge states of fragment particles,[13–17] and (4) other things.[18–20] There are a lot of works on the multiple ionization of monoatomic targets.[21–29] Regarding the molecular targets, the dependence of the multiple ionization cross sections on the incident beam direction were investigated for a H_2 target, induced by the proton impact[6,7] and by the O^{8+} impact.[8] Kabachnik *et al.*[9] and Siegmann *et al.*[10] measured the ionization cross sections of a N_2 target, where the correlation with the incident-direction was found. The orientation dependence of the ionization cross section was also reported for the CO target, bombarded by the 96 MeV Ar^{14+} ions.[11] Using the coincidence time-of-flight (TOF) technique, the fragment ions, originating from the CO molecule, were measured under the 1 MeV/u F^{4+} impact,[13,14] the 1 MeV/u F^{6+} impact,[15] and the 97 MeV Ar^{14+} impact.[16] Ben-Itzhak *et al.*[13] reported in detail the fragmentation pattern of a decay $(CO)^{q+} \rightarrow C^{i+} + O^{j+}$ $(i + j = q)$ as well as the charge states, i and j, of the dissociated ions.

On the multiple ionization process, several theoretical models were well known so far. They have a common feature that the impact-parameter-dependent ionization probability in the independent electron picture plays a dominant role. At first those models were developed to treat the excitation of multi-electron single-atom targets, but recently they were also applied to the multi-atom systems. One is the statistical energy deposition model (SEDM),[9,10,30–33] developed by Russek *et al.*[30] Based on the SEDM, Kabachnik *et al.*[9] studied the molecular orientation effect in the multiple ionization of a N_2 target, bombarded by the 200 keV He^+ ion. Here they reported that with increasing the recoil-ion charge state the multiple ionization cross section strongly depends on the angle between the beam direction and the molecular axis. There, they estimated the deposited energy as the impact-parameter-dependent energy loss values of the ion, calculated in the framework of the dielectric function method. It is noted that the key factor (we call g-factor) in the SEDM, which characterizes the transition probability, cannot be estimated in this theory itself so that it has been treated as a free parameter.

Another model is the independent-electron-model (IEM),[21–27] in which the electron–electron interaction is ignored and all of the electrons in an ensemble are equivalently treated. When this model is applied to the multiple ionization process, we need the one-electron ionization probability $P(b)$ as a function of impact parameter b. However, except for incident ions in low charge states, the theoretically derived $P(b)$ often exceeds unity.[27,28] In this case some artificial re-difinition was inevitable in order to use $P(b)$ as the probability. On the other hand, from the experimental viewpoints, the expression $P(b) = \alpha \exp(-\beta b)$ was often adopted. Here α and β are the parameters, which are chosen to reproduce the experimental data as well as possible.[22,24,25,34]

Recently we developed a model for the $P(b)$ that is not greater than unity even in the incidence of highly charged ions.[35] A comprehensive study with the use of this $P(b)$ reveals that the multiple ionization cross sections of a single-atom target induced by swift ion impacts could be well reproduced.[35] The aim of the present paper is to extend the recently developed model to the multiple ionization process of the molecular targets. In §2, we describe the theoretical model. There we prove the sum rule on the net ionization cross section. Section 3 is devoted to the presention of the numerical results together with comparison with the available experimental data. Discussion will be also given there. Throughout the paper, e, m, a_B, v_B and $\hbar$ denote the elementary electric charge, the electron rest mass, the Bohr radius, the Bohr velocity and the Planck constant divided by 2π, respectively.

2. Theoretical Models

2.1 Contracted independent electron model (CIEM)

We consider the multiple ionization process of the molecular targets by the fast ion impact in the energy range over several ten keV/u (but non-relativistic). There the speed of the ion is much greater than those of the vibrational and the rotational motions of a molecule, so that we may neglect those motions and we assume the constituent nuclei to be frozen at the positions in the ground state during the collision. In addition, we regard the diatomic targets as two neutral atoms with the separation of the interatomic distance of the molecule being kept constant. Then the character of a molecule is featured by the spatial correlation of two atoms. Here we consider the case where the ion speed is so high that the target electrons are excited directly (not adiabatically). In addition, as seen later, the ionization probability $P(b)$ rapidly decreases with the impact-parameter b increasing. Then we may investigate the ionization of a molecule in the picture of an isolated-atom ensemble. In this case, the key quantities are the successive ionization potentials and the internuclear separations of the constituent atoms. We consider the multiple ionization process in the independent electron model (IEM).

First we consider the case of a single-atom target for simplicity. In the conventional IEM, the orbital energies of a neutral atom were often employed. In this case, the ionization potentials do not depend on the degree of ionization. In the previous study,[35] we showed that this method often presented the unreasonable q (recoil charge)-dependences of the multiple ionization cross section. Therefore we adopted the CIEM, where the successive ionization potentials depend on the one-by-one removal of an electron. We assume that the ionization starts from the outermost electron shell. The n-th ($n = 0, 1, 2, \ldots$) multiple ionization probability in the CIEM is expressed with the i-th ionization potential ϵ_i ($i = 1, 2, \ldots$) as

$$P_0(b) = C(1 - P(b, \epsilon_1))^N,$$
$$P_n(b) = C\binom{N}{n}\left\{\prod_{i=1}^{n} P(b, \epsilon_i)\right\}(1 - P(b, \epsilon_{n+1}))^{N-n} \quad (n = 1, 2, \ldots) \tag{1}$$

where N is the total number of electrons in the shell to which the ionized electrons belong. In eq. (1), The electronic shells are characterized only by the principal quantum numbers. Also n ($\leq N$) is the number of ionized electrons, and C denotes the normalization constant to be determined by satisfying $\sum_{n=0}^{n=N} P_n(b) = 1$. The n-th ionization cross section σ_n and the net ionization cross section $\sigma_{\rm net}$ are expressed as

$$\sigma_n = 2\pi \int_0^\infty \mathrm{d}b\, bP_n(b), \quad \sigma_{\rm net} = \sum_n n \times \sigma_n. \tag{2}$$

Let us extend this treatment to a diatomic molecular target. An extension to multi-atom targets are straightforward. Here we suppose that two homonuclear isolated atoms locate on the xz plane at an equilibrium distance l. The position vectors of those atoms are given in Cartesian coordinates by $(-\frac{l}{2}\sin\theta, 0, \frac{l}{2}\cos\theta)$ and $(\frac{l}{2}\sin\theta, 0, -\frac{l}{2}\cos\theta)$. Here θ is the angle between the z axis and the molecular axis. In the frame of the IEM, the impact-parameter-dependent ionization probability for such a diatomic target is formulated as

$$P_n(\boldsymbol{b}, \theta) = \sum_{j=0}^{n} P_{n-j}^{\alpha}(b_\alpha) P_j^{\beta}(b_\beta), \tag{3}$$

where P_{n-j}^{α} (P_j^{β}) denotes the $(n-j)$-th (j-th) ionization probability of the α (β) atom. We assume that the incident ion moves along a straight-line, parallel to the z axis. The b_α and b_β denote the impact-parameters referring to the atoms α and β in the molecule, respectively. Then we have

$$b_\alpha = \sqrt{\left(b_x - \frac{l}{2}\sin\theta\right)^2 + b_y^2}$$

and

$$b_\beta = \sqrt{\left(b_x + \frac{l}{2}\sin\theta\right)^2 + b_y^2}.$$

By averaging the θ-dependent ionization cross section over the solid angle $\mathrm{d}\Omega = 2\pi\sin\theta \mathrm{d}\theta$, we obtain the averaged multiple ionization cross section of the form

$$\sigma_n = \frac{\int \mathrm{d}\Omega \int \mathrm{d}\boldsymbol{b} P_n(\boldsymbol{b}, \theta)}{\int \mathrm{d}\Omega}. \tag{4}$$

The differential multiple ionization cross section is then defined by

$$\frac{\mathrm{d}\sigma_n}{\mathrm{d}\theta} = \frac{\sin\theta}{2} \int \mathrm{d}\boldsymbol{b} P_n(\boldsymbol{b}, \theta). \tag{5}$$

Later, we will discuss the molecular effect in the multiple ionization process of a molecular target on the basis of eqs. (3)–(5).

2.2 Modeled ionization probability

Let us start with a brief description of the modeled one-electron ionization probability $P(b)$ as a function of impact parameter b. More details on the derivation were described in another paper.[35] Our procedure is the followings: (1) the ionized electron is described by a hydrogenic 1s orbital with the effective binding charge $Z_{\rm e}$ and the orbital parameter are determined by $Z_{\rm e}$. (2) we adopt the differential ionization cross section in Born approximation per unit kinetic energy of the ionized electron. (3) the impact parameter dependence of $P(b)$ is introduced through the accurate expression for the energy transfer to the electron in the classical free collision.

Here we describe the theoretical model briefly. Let us consider the single electron ionization process of the target bombarded by a swift charge in the frame of the Born approximation. The electron is assumed to be initially in the hydrogen-like state with the effective charge $Z_{\rm e}$ and the orbital-size parameter a, which are determined by the binding energy ϵ as $Z_{\rm e} = (2\hbar^2/me^4 \times \epsilon)^{1/2}$ and $a = a_{\rm B}/Z_{\rm e}$. Then, we assume the initial-state wavefunction to be a hydrogenic 1s state as $\psi_{1s}(r) = (\pi a^3)^{-1/2}\exp(-\frac{r}{a})$. On the other hand, the final-state wavefunction is described by

$$\psi_{\boldsymbol{\kappa}}(r) = (2\pi)^{-3/2} \mathrm{e}^{\pi/2a\kappa} \Gamma\left(1 + \frac{\mathrm{i}}{a\kappa}\right) \times \mathrm{e}^{\mathrm{i}\boldsymbol{\kappa r}} F\left(-\frac{\mathrm{i}}{a\kappa}, 1, -\mathrm{i}(\kappa r + \boldsymbol{\kappa r})\right).$$

Here $F(-\frac{\mathrm{i}}{a\kappa}, 1, -\mathrm{i}(\kappa r + \boldsymbol{\kappa r}))$ is a confluent hypergeometric function.[36] Here the initial-state and the final-state wavefunctions are orthogonal since those are the eigenfunctions of the same Schroedinger equation, belonging to different eigenenergies. The final-state wavefunction includes the distortion due to the residual coulomb field. According to a quantum-mechanical treatment,[36] the differential ionization cross section of the hydrogen-like atom bombarded by a swift charge $Z_1 e$ at a speed v relative to the electron is expressed in the following form:

$$\frac{\mathrm{d}^2\sigma_{\mathrm{ion}}}{\mathrm{d}K\,\mathrm{d}Q} = 8\pi a_{\mathrm{B}}^2 \left(\frac{Z_1 v_{\mathrm{B}}}{Z_{\mathrm{e}} v}\right)^2 \frac{K}{Q} \frac{2^8 \exp\left[-\frac{2}{K}\arctan\frac{2K}{1-K^2+Q^2}\right]}{[1+(K+Q)^2]^3[1+(K-Q)^2]^3} \times \frac{Q^2+\frac{1}{3}(1+K^2)}{1-\exp\left(-\frac{2\pi}{K}\right)} \tag{6}$$

Here, we introduced the non-dimensional reduced variables $K \equiv \kappa a_{\mathrm{B}}/Z_{\mathrm{e}}$ and $Q \equiv q a_{\mathrm{B}}/Z_{\mathrm{e}}$, instead of the wavenumber of the ionized electron, κ, and the magnitude of the momentum transfer, q. Now the case is considered where the kinetic energy of the projectile is greater than that of the ionized electron. Then the differential ionization cross section per unit interval of K is given as

$$\frac{\mathrm{d}\sigma_{\mathrm{ion}}}{\mathrm{d}K} = \int_{Q_{\min}(K)}^{Q_{\max}} \mathrm{d}Q\, \frac{\mathrm{d}^2\sigma_{\mathrm{ion}}}{\mathrm{d}K\,\mathrm{d}Q}, \tag{7}$$

where $Q_{\min}(K) = (K^2+1)/(2V)$, $Q_{\max} = 2\mu V/(m)$, $V = v/(Z_{\mathrm{e}} v_{\mathrm{B}})$ and μ is the reduced mass.

Next, we introduce the impact-parameter dependence of the energy transfer in a classical manner. This is motivated by the fact that the classical picture in the energy loss is valid especially for a highly charged ions in collision with an electron. Now we consider that the speed of the projectile is great enough so that the binding effect of the bound electron is ignored. Then the electron is assumed to be at rest at the nucleus position. In addition, according to quantum-mechanics, the average (or expectation) value, $\langle \boldsymbol{r} \rangle = \int \mathrm{d}\boldsymbol{r}\, \boldsymbol{r} |\psi(\boldsymbol{r})|^2$, of the position vector $\boldsymbol{r}$ for an atomic electron is vanishing. Then the bound electron is assumed to be initially at the nucleus position. Here, the nuclear charge does not play any role except as the binding center.[37] The ion trajectory is well described by a straight-line so that the impact parameter of the ion trajectory with respect to the target nucleus is the same as that in the ion–electron collision. We treat the energy transfer to the electron in the rigorous Rutherford scattering picture. Now this picture successfully treats the electronic energy-loss of swift ions in materials. According to the accurate coulomb scattering formula,[38] the transferred energy $\Delta E(b)$ is given by

$$\Delta E(b) = \frac{2Z_1^2 e^4}{mv^2} \frac{1}{b^2 + (Z_1 e^2/mv^2)^2}. \tag{8}$$

It is noted that the maximum energy transfer $\Delta E_{\max}$ is given by $2mv^2$, occurring at $b = 0$. The existence of $\Delta E_{\max}$ is well-known as the binary peak in the energy spectra of the secondary electrons in the head-on collision geometry.[39] It is remarkable that $\Delta E_{\max}$ is independent of the magnitude of the incident charge. We keep in mind that though the energy transfer is treated classically, the spatial spread of the bound electron cloud is already taken into account in the quantum-mechanical way in eq. (7).

Let us combine $\Delta E(b)$ with the differential ionization cross section. Under the condition we assume, we are allowed to regard $\Delta E(b)$ as the kinetic energy $\hbar^2\kappa^2/(2m)$ of the ionized electron. Thus, the resultant wavenumber κ of the ionized electron is expressed as a function of b. We define the reduced wavenumber $K(b) = \kappa(b) \times a_{\mathrm{B}}/Z_{\mathrm{e}} = (2mva/\hbar)(A/\sqrt{b^2+A^2})$ with $A = Z_1 e^2/(mv^2)$. Making use of the expression of $K(b)$ and eq. (7), we request $P(b,\epsilon)$ to lead the expression of σ_{ion}, which is derived from (6), Then we can uniquely determine

$$P(b,\epsilon) = [K(b)]^4 \int_{Q_{\min}}^{Q_{\max}} \frac{\mathrm{d}Q}{Q} \frac{Q^2+\frac{1}{3}(1+K(b)^2)}{1-\exp\left(-\frac{2\pi}{K(b)}\right)} \times \frac{2^8 \exp\left[-\frac{2}{K(b)}\arctan\frac{2K(b)}{1-K(b)^2+Q^2}\right]}{[1+(K(b)+Q)^2]^3[1+(K(b)-Q)^2]^3}, \tag{9}$$

where the ϵ-dependence is brought via the orbital parameter a, which is included in $K(b)$. In fact one can see that $P(b,\epsilon)$ leads to

$$\sigma_{\mathrm{ion}} = 2\pi \int_0^\infty \mathrm{d}b\, bP(b,\epsilon) = \int_0^{K_m} \mathrm{d}K \int_{Q_{\min}}^{Q_{\max}} \frac{\mathrm{d}^2\sigma_{\mathrm{ion}}}{\mathrm{d}K\,\mathrm{d}Q},$$

with $K_m = 2V$. This cross section is proportional to the square charge of the incident ion, and equivalent to the quantum-mechanical ionization cross section in the Born approximation, except for the difference in the upper limit of K-integral. However, this difference is substantially of no importance as far as the ion speed is not so small.

Here we remark that $P(b,\epsilon)$ and σ_{ion} satisfy the scaling laws. To make clear the dependences on the physical parameters, we denote $P(b,\epsilon)$ in eq. (9) as $P(b, v, Z_1, Z_{\mathrm{e}})$. Defining the reduced impact parameter $\tilde{b}$ and the reduced speed $\tilde{v}$ by $\tilde{b} \equiv Z_{\mathrm{e}}^2 b/Z_1$ and $\tilde{v} \equiv v/Z_{\mathrm{e}}$, respectively, we can prove the scaling rule:

$$P(b, v, Z_1, Z_{\mathrm{e}}) = P(\tilde{b}, \tilde{v}, 1, 1). \tag{10}$$

Here $P(\tilde{b}, \tilde{v}, 1, 1)$ means the ionization probability of a hydrogen atom in collision with an incident proton moving at a speed $\tilde{v}$ along a straight-line trajectory at an impact parameter $\tilde{b}$. This scaling relation guarantees that the $P(b, v, Z_1, Z_{\mathrm{e}})$ has a meaning of absolute probability as far as $P(\tilde{b}, \tilde{v}, 1, 1)$ does not exceed unity. If we write the corresponding ionization cross section as $\sigma_{\mathrm{ion}} \equiv \sigma_{\mathrm{ion}}(v, Z_1, Z_{\mathrm{e}})$, one immediately finds another scaling relation

$$\sigma_{\mathrm{ion}}(v, Z_1, Z_{\mathrm{e}}) = (Z_1/Z_{\mathrm{e}}^2)^2 \sigma_{\mathrm{ion}}(\tilde{v}, 1, 1), \tag{11}$$

where $\sigma_{\mathrm{ion}}(\tilde{v}, 1, 1) = 2\pi \int_0^\infty \mathrm{d}\tilde{b}\, \tilde{b} P(\tilde{b}, \tilde{v}, 1, 1)$. It is worthwhile to note that the present and the first-Born ionization cross sections are both scaled by the same scale variables, while the scaling law of the $P(b,\epsilon)$ is different from each other. We should remark that the $P(b,\epsilon)$ in the first Born approximation grows up as Z_1^2 as far as the other variables are kept unchanged. Consequently, for large Z_1, the value of $P(b,\epsilon)$ will be in fact greater than unity especially at a small b. On the contrary, in our case the prefactor of the scaled

probability is just unity, as shown in eq. (10), so that $P(b,\epsilon)$ is not over unity for any allowed b, irrespective of Z_1.

As a final part of this section, we give an approximate form for $P(b,\epsilon)$. At a high speed, the integrand in $P(b,\epsilon)$ has a dominant contribution from a region $Q \approx K(b)$, so that $\arctan[2K(b)/1-K(b)^2+Q^2]$ and $[1+(K(b)+Q)^2]^3$ in eq. (9) approximates $\arctan 2K(b)$ and $[1+4(K(b))^2]^3$, respectively. After this replacement, the integration over Q leads to an analytical approximation $P_{\rm ap}(b,\epsilon)$:

$$P_{\rm ap}(b,\epsilon) \equiv \frac{2^7 K(b)^4 \exp\left\{-\frac{2}{K(b)}\arctan 2K(b)\right\}}{3(4K(b)^2+1)^3(1-{\rm e}^{-2\pi/K(b)})} \times \left[\frac{3K(b)^5+7K(b)^3+6K(b)}{(1+K(b)^2)^2}\left\{\frac{\pi}{2}-\arctan Q_0\right\} - \frac{1}{(1+K(b)^2)^2}\log\frac{(Q_0+K(b))^2}{Q_0^2+1} - \frac{(3K(b)^3+4K(b))Q_0+1}{(1+K(b)^2)(Q_0^2+1)} - \frac{2K(b)Q_0-1}{(Q_0^2+1)^2}\right], \tag{12}$$

where $Q_0 = Q_{\rm min} - K(b)$. Comparison with the $P(b,\epsilon)$ in eq. (9) will be made later.

2.3 *Sum rule on net ionization cross section*

Here we prove the sum rule on the net ionization cross section of molecular targets under the assumption of the isolated-atom picture. Let n_t denote the number of bound electrons in the t atom ($t=\alpha,\beta$). In addition, we set $n_c = n_\alpha + n_\beta$, and use the abbreviations P_j^α and P_j^β for $P_j^\alpha(b_\alpha)$ and $P_j^\beta(b_\beta)$ ($j=0,1,2,\ldots$), respectively. With the use of the normalization $\sum_{j=0}^{n_t} P_j^t = 1$ ($t=\alpha,\beta$) and the expression (3), one obtains

$$\sum_{n=1}^{n_c} nP_n(b) = \sum_{k=1}^{n_\beta} kP_k^\beta + \sum_{k=1}^{n_\alpha} kP_k^\alpha, \tag{13}$$

Integrating the above equation over $2\pi b\,{\rm d}b$, one finally proves the additive rule on the net ionization cross section such that

$$\sigma_{\rm net}^{\alpha+\beta} = \sigma_{\rm net}^\alpha + \sigma_{\rm net}^\beta. \tag{14}$$

We remark that the above relation is exactly valid, as far as we take the picture that the molecule system is regarded as the ensemble of isolated atoms. In this picture, the validity of the above sum rule is independent of what kind of the ionization potentials we adopt. Moreover, this sum rule can be straightforwardly proved for the multi-atom targets in a similar manner.

2.4 *Statistical energy deposition model (SEDM)*

As another theoretical model, we briefly describe the statistical energy deposition model (SEDM). Later, comparison will be made with the CIEM results and the experimental data. In this model, the energy transferred from the incident ion to the target electrons will be consumed in the multiple ionization via the auto-ionizing excitations. According to Russek *et al.*,[30] the probability of n-th fold ionization in the system composed of N equivalent electrons is given by

$$P_n^N = \frac{\binom{N}{n} g^n S_n(E_k)}{\sum_{j=1}^{N}\binom{N}{j} g^j S_j(E_k)}, \qquad S_j(E) = 2^{[(j-1)/2]}\pi^{[j/2]}E^{(3j-2)/2}/(3j-2)!!, \tag{15}$$

where $[\alpha]$ means the integral part of a real number α. In addition, $E_k = E_{\rm T} - \sum_i \epsilon_i - E_{\rm R}(n)$ denotes the kinetic energy available for the ionized electrons, ϵ_i is the i-th binding energy of an electron, $E_{\rm R}(n)$ is the energy given to a residual ion, and $E_{\rm T}$ is the total energy deposited by the projectile. Here g is a fitting parameter, appropriately chosen for a problem. In addition, $S_j(E)$ comes from the final density of states for the case of n electrons sharing the kinetic energy E in the continuum. Usually, the deposited energy $E_{\rm T}(b)$ is calculated as a function of the impact parameter b by means of the stopping force in the dielectric function formalism. Thus we have

$$E_{\rm T}(b) = \int_{-\infty}^{\infty} {\rm d}z\left(\frac{{\rm d}E(r)}{{\rm d}z}\right), \tag{16}$$

where $r=\sqrt{b^2+z^2}$. Here we assume that the ion moves at a constant speed v on a straight-line trajectory, parallel to the z-axis at an impact parameter b. The local stopping force is expressed as

$$\frac{{\rm d}E(r)}{{\rm d}z} = \frac{2(Z_1 e)^2}{\pi v^2}\int_0^\infty \frac{{\rm d}k}{k}\int_0^{kv} {\rm d}\omega\,\omega\Im\left[\frac{-1}{\epsilon(k,\omega,\rho(r))}\right]. \tag{17}$$

Here $\epsilon(k,\omega,\rho(r))$ denotes the dielectric function of a target material, obtained by substituting the local electron density $\rho(r)$ into the constant electron density ρ_0 in the expression of Lindhard dielectric function $\epsilon(k,\omega)$. By this replacement, we introduce the locality in the corresponding quantities such as the local Fermi velocity $v_{\rm F}(r) = \hbar(3\pi^2\rho(r))^{1/3}/m$, the local plasma frequency $\omega_{\rm p}(r) = (e^2\rho(r)/\epsilon_0 m)^{1/2}$, etc. The stopping cross sections, obtained by summing up the local stopping force over the spatial volume per atom, are known to yield good agreement with the data, especially at higher impact energies (*e.g.*, 100 keV for a proton).[40] Later, we will show the SEDM results, evaluated on the basis of our treatment[40] with inclusion of the energy straggling.[41]

3. Numerical Results and Discussion

First we show the results for the b-dependent ionization probability. Figure 1 shows the $P(b,\epsilon)$ of eq. (9) (the solid line) and the approximate form $P_{\rm ap}(b,\epsilon)$ of eq. (12) (the dotted line) for a hydrogen atom, bombarded by the 1 MeV proton. Also the corresponding ionization cross sections, $\sigma_{\rm ion}$ and $\sigma_{\rm ion,ap}$, calculated from $P(b,\epsilon)$ and $P_{\rm ap}(b,\epsilon)$ are drawn in Fig. 2. At a lower speed, the latter cross section is larger than the former. Nevertheless, this approximation yields the overall agreement in both $P(b,\epsilon)$ and $\sigma_{\rm ion}$ over the range of the incident energy studied.

Before showing the calculated results, we explain how to choose N and how to obtain $P_n(b)$ of eq. (1). For a nitrogen atom, as an example, we discern the electronic shell only by the principal quantum number so that $N=5$ and 2 for the L-shell and the K-shell, respectively. Ionization will start from the L-shell. For the single ionization, we have $P_1(b) = C\binom{5}{1}P(\epsilon_1)(1-P(\epsilon_2))^4$, where the variable b in $P(b,\epsilon)$ is

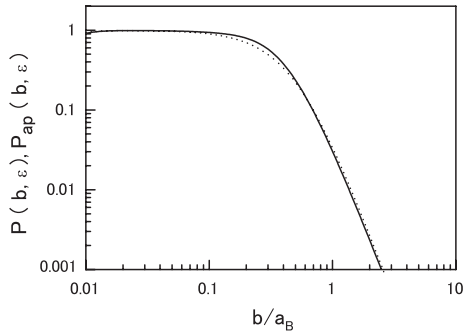

Fig. 1. $P(b,\epsilon)$ of eq. (9) (solid line) and $P_{ap}(b,\epsilon)$ of eq. (12) (dotted line) for a hydrogen atom ($\epsilon = 0.5$ a.u.) by the 1MeV proton impact, as a function of the impact parameter b. Here a.u. means the atomic units.

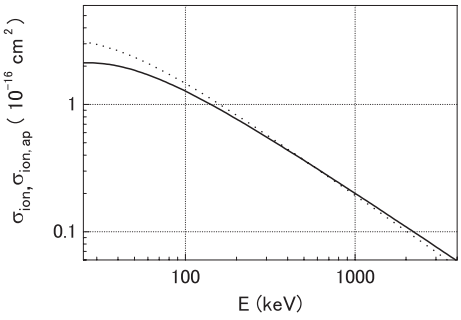

Fig. 2. σ_{ion} (solid line) and $\sigma_{ion,ap}$ (dotted line), calculated respectively from $P(b,\epsilon)$ and $P_{ap}(b,\epsilon)$ for a hydrogen atom by the impact of $Z_1 = 1$, as a function of the projectile's kinetic energy.

omitted. For the 6-fold ionization, the L-shell electrons are completely ionized, and one of the K-shell electrons is also ionized. Then we have $P_6(b) = C\binom{5}{5}\prod_{i=1}^{5} P(\epsilon_i)\binom{2}{1}P(\epsilon_6)(1 - P(\epsilon_7))$. Figures 3(a)–3(d) show the $d\sigma_n/d\theta$ in eq. (5) of a N_2 molecule by the 200 keV He^+ ion impact as a function of the angle θ between the molecular axis and the incident beam direction. Here, (a)–(d) correspond to the cases of $n = 2$–5, respectively. When applying $P(b,\epsilon)$ to the CIEM, we employed the data on the successive ionization energies[42] listed in Table I. For comparison, the calculation based on the SEDM was carried out under the same condition of $g = 0.1$ as Kabachnik *et al.*[9] adopted. The electron density of the molecule is calculated using the molecular-orbital wave functions.[43] The inter-atomic separation l of a N_2 molecule is assumed to be $2.068a_B$.[44] In the figure, the solid lines, the broken lines, the histograms, and the chain lines denote the CIEM results, the SEDM results,

Table I. Binding energies of electrons in eV for N, C, and O targets.[42]

Target \ n	1	2	3	4	5	6	7	8
N	14.534	29.601	47.448	77.742	97.863	552.057	667.029	
C	11.260	24.383	47.887	64.492	392.077	489.983		
O	13.618	35.116	54.934	77.412	113.896	138.116	739.315	871.390

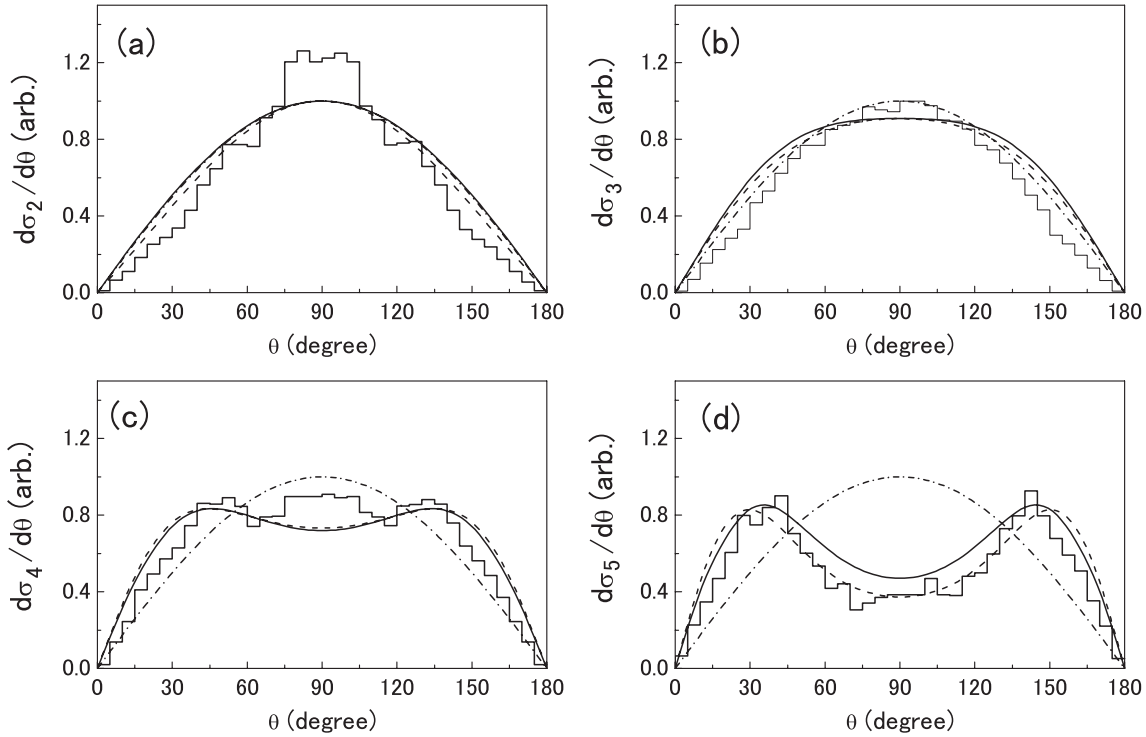

Fig. 3. $d\sigma_n/d\theta$ of a N_2 molecule by the 200 keV He^+ ion impact as a function of θ for the degree of ionization: (a) $n = 2$, (b) $n = 3$, (c) $n = 4$, and (d) $n = 5$. The solid lines and the broken lines denote the CIEM results and the SEDM ($g = 0.1$) results, respectively. The dot-dash lines indicate the $\sin\theta$-curves. The experimental data[9] are indicated by histograms.

the experimental data, and the $\sin\theta$-curve, respectively. The units of the ordinates are in arbitrary units. The deviation from the $\sin\theta$-curve represents the beam direction dependence. Because the $d\sigma_2/d\theta$ in the CIEM and in the SEDM agree with the $\sin\theta$-curves, that is, the integral part in eq. (5) for $n = 2$ is roughly independent of θ. With increasing the value of n, the $d\sigma_n/d\theta$ around $\theta = 90^\circ$ tends to be smaller than the $\sin\theta$-curves. It means that the θ-dependence of the differential cross section becomes strong. On the other hand, around $\theta = 0^\circ$, σ_n is larger than the $\sin\theta$-curve. This is because the multiple ionization cross section for the large q cases tends to dominate at small impact parameters with respect to each atom. Here we summarize that the results from the CIEM and from the SEDM with $g = 0.1$ tend to be close each other, and both models qualitatively reproduce the experimental data. There is a suggestion[9] that the deviations of the experimental data from the $\sin\theta$-curve, appearing around $\theta = 90^\circ$ in Figs. 3(a) and 3(c), are due to the transfer ionization. We find that our SEDM results look very similar to those calculated by Kabachnik *et al.*[9] Finally we note that the CIEM reflects the molecular orientation effect rather well without introducing any fitting parameters. This is a contrast to the case of the SEDM analysis, that requests g to serve as a fitting parameter.

Figure 4 shows the energy dependence of the multiple ionization cross section σ_n *per atom*, calculated in the CIEM and in the SEDM, for a N_2 molecule target by the H^+ impact. The solid line and the dash-dot line denote the CIEM results and the SEDM ones with $g = 0.05$, respectively. The choice of $g = 0.05$ is to follow Kabachnik *et al.*[4] The open squares[1] denote the direct (without capture process) ionization cross section for $n = 1$, and the open circles[44] and the solid squares[1] indicate the experimental data on σ_n without excluding the electron capture contribution. Compared with the CIEM results, the energy dependence of the SEDM results is rather weaker. In particular, for $n = 1$ the SEDM results seem to be in good agreement with the experimental data as long as the energy range less than 500 keV is considered. However, we must take care that at high energies these experimental data overestimate the direct ionization component because they include the electron capture contribution. In fact, if we restrict the data at the energies of more than 1 MeV, the energy dependence of the CIEM results looks better than the SEDM. The main reason why the SEDM results tend to agree with the data is due to the appropriate selection of the fitting parameter g, the dependences of which on the physical parameters are not clear.

Figure 5 shows the CIEM results on σ_n ($n = 1$–4) under the proton impact for a N atom target and for a N_2 molecule target. The thick solid line indicates the net ionization cross section σ_{net}. The thin solid lines and the dotted lines show the σ_n *per atom* for atomic and molecular targets, respectively. The values of n are indicated near the corresponding curves. The open squares denote the experimental data[1] on the σ_1 for a N_2 molecule target with excluding the capture process. As an overall feature, one finds the decreasing tendency of the σ_n at high incident energies. On the other hand, at lower incident energies, the σ_n for higher charge components ($n = 3, 4$) tend to decrease. It is remarkable that the σ_1 *per atom* for a molecular target is less than that for an atomic target at given energies. On the contrary, this is not the case for the higher charge states $n = 2$–4. This result is understood from the sum rule on the net ionization cross section. According to the sum rule, at a certain incident energy, the increase of σ_n *per atom* for $n = 2$–4 has to be compensated by the decrease of σ_1. The appearance of the increase or the decrease in the ionization cross section per atom is called the molecular effect. This is due to the existence of target atoms in the vicinage. The molecular

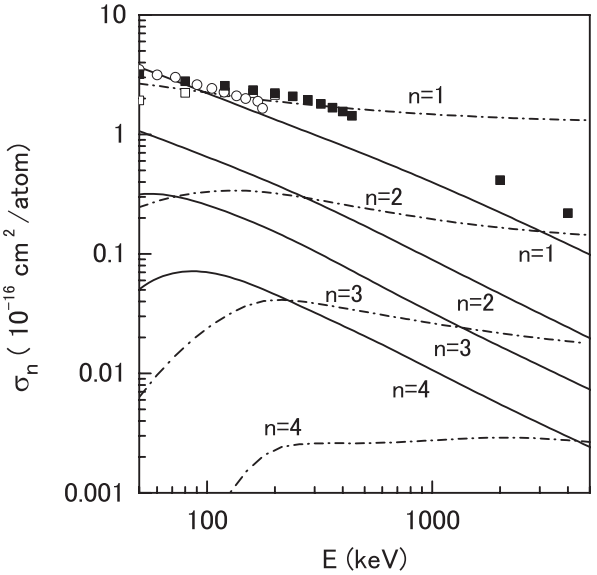

Fig. 4. σ_n *per atom* of a N_2 molecule target as a function of the incident H^+ energy. The solid lines denote the CIEM results of σ_n ($n = 1$–4) for a N_2 target, and the dot-dash lines are the SEDM results ($g = 0.05$) of σ_n ($n = 1$–4) for a N_2 target. The open squares denote the experimental data on the σ_1[1] without the electron capture process. The solid squares[1] and the open circles[44] are the data including the electron capture process.

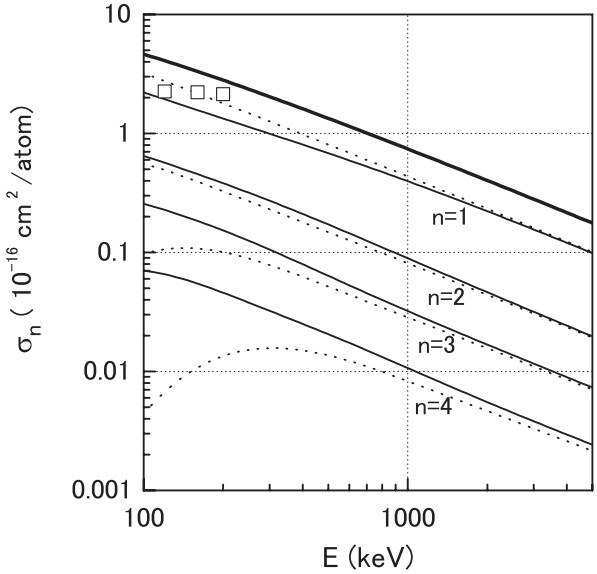

Fig. 5. σ_n *per atom* of a N target and of a N_2 molecule target calculated in the CIEM as a function of the incident proton energy. The thick solid line indicates the *net* ionization cross section σ_{net}. The thin solid lines and the broken lines denote, respectively, σ_n ($n = 1$–4) for a N_2 target and for a N target. The open squares denote the experimental data on the σ_1 for a N_2 target.[1]

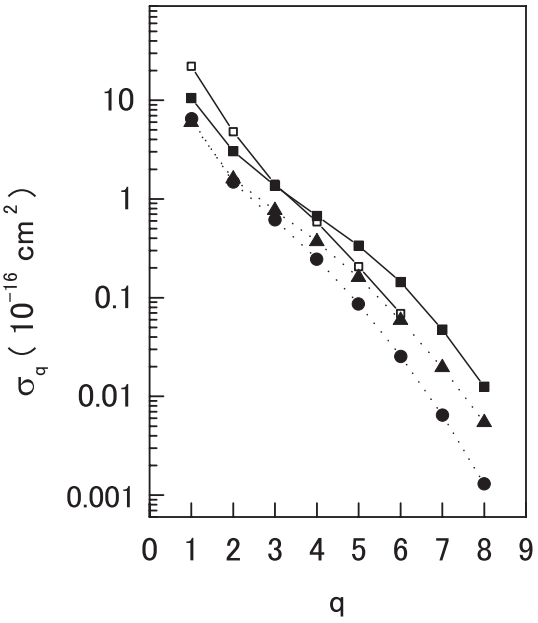

Fig. 6. σ_q vs q for producing a $(CO)^{q+}$ ion by the 1 MeV/u F^{4+} impact. The open squares and the solid squares denote the experimental data[13] and the CIEM results, respectively. The solid circles and the solid triangles denote the SEDM results for $g = 0.01$ and for $g = 0.02$, respectively. The solid and broken lines are drawn only to guide the eyes.

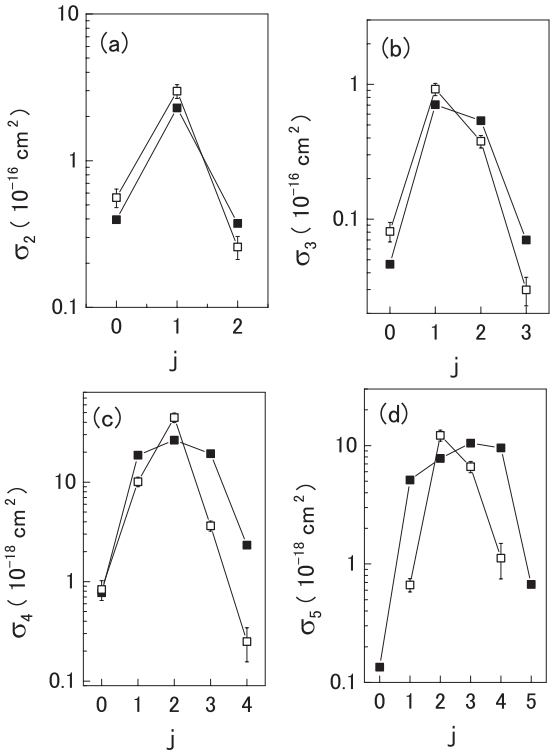

Fig. 7. σ_q vs j for producing a O^{j+}, fragmented from a $(CO)^{q+}$ by the 1 MeV/u F^{4+} impact: (a) $q = 2$, (b) $q = 3$, (c) $q = 4$, (d) $q = 5$. The solid squares denote the CIEM results and the open squares with error bars denote the experimental data.[13]

effect becomes smaller with increasing the incident energy.

Regarding the multiple ionization process of the heteromolecule CO, Ben-Itzhak *et al.*[13] investigated the following dissociation process by F^{4+} impact:

$$(CO)^{q+} \longrightarrow C^{i+} + O^{j+} \quad (q = i + j). \tag{18}$$

They measured the relative abundances of the final products indicated in the right-hand side of eq. (18), and obtained the relative cross section for the fragmentation pattern. We also apply the CIEM to this system. Figure 6 shows the q-fold ionization cross section σ_q for a CO molecule target induced by the 1 MeV/u F^{4+} incidence. The abscissa indicates the total recoil charge q $(= i + j)$ produced in the above reaction. The open squares and the solid squares denote, respectively, the experimental data,[13] and the CIEM results. For comparison, we draw the SEDM results for $g = 0.01$ and 0.02 by the solid circles and the solid triangles, respectively. In representing the experimental data, we determined the corresponding cross sections by multiplying the relative abundances to a $(CO)^+$ product by the production cross section[13] of a $(CO)^+$, $\sigma\ (CO^+) = (1.7 \pm 0.8) \times 10^{-15}\,\mathrm{cm}^2$. In the SEDM results, the selection of $g = 0.02$ yields much better agreement with the experimental data. In order to display to what extent the g-value affects the multiple ionization cross section, we also plot the results for $g = 0.01$. From these two curves, one sees that the variation of g value improves the σ_q at higher charge states, while at the lowest charge state there comes no significant change. This is a typical feature of the SEDM. Namely, the ionization cross sections for the low charge states are nearly independent of the magnitude of g value. The detailed comments on this point were given in the previous research.[35] Anyway, both the CIEM and the SEDM $(g = 0.02)$ yield good agreement with the experimental data, and there is not so large difference in these theoretical results. However, we would like to stress that any fitting parameters are not incorporated in the CIEM calculation.

Figure 7 shows the cross section σ_q for producing O^{j+} ions and C^{i+} ions, fragmented from the $(CO)^{q+}$ ions, directly produced by the 1 MeV/u F^{4+} impact. Here Figs. 7(a)–7(d) correspond to the case of $q = 2$–5, respectively, where $q = i + j$. In these figures, the open squares denote the experimental data[13] and the solid squares denote the CIEM results. Ben-Itzhak *et al.*[13] reported that 94.0% of $(CO)^{2+}$ ions were dissociated. Therefore we may assume that all of the ionized molecules produced in the collision will fragment into C^{i+} and O^{j+} ions. The figure shows that the charge symmetry condition $(i \approx j)$ looks preferential. In order to see this in detail, we show in Fig. 8 the orientation-averaged differential cross section per unit impact parameter, $\mathrm{d}\sigma/\mathrm{d}b$ $[= 2\pi b P(b)]$, for the case of $q = 4$ $(j = 0$–$4)$ as a function of b. Here b is measured from the position of the oxygen nucleus. One can see that with increasing the charge j, the peak position of $\mathrm{d}\sigma/\mathrm{d}b$ shifts closer toward the oxygen nucleus. It is easy to understand that the values of $\mathrm{d}\sigma/\mathrm{d}b$ are very small at $j = 0$ and $j = 4$. Because $\mathrm{d}\sigma/\mathrm{d}b$ at $j = 0$ is contributed from the product of $P(b)$ for producing the oxygen ion in the $j = 0$ state and $P(b)$ for producing the carbon ion in the $i = 4$ state. The latter $P(b)$ is localized around the carbon nucleus so that the overlap of them becomes very small, though the former value is relatively large. In turn, in other cases the product of two quantities amounts to be relatively large. For the cases of $q = 4$ and 5, the experimental values have a peak around $i = j$, while the calculated results display a bit broad peak. One possibility to explain this feature is that an extremely asymmetric

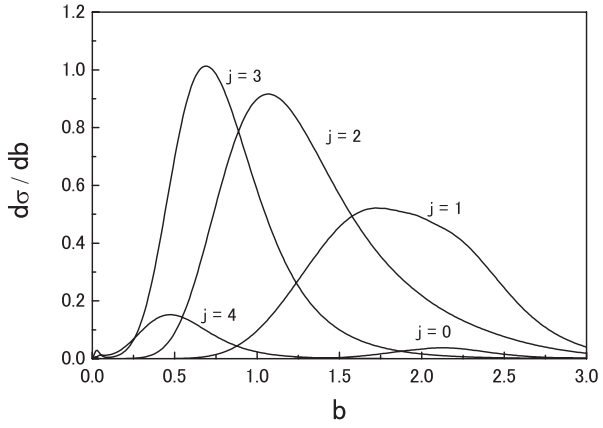

Fig. 8. $d\sigma/db$ vs b for producing a O^{j+} ($j = 0$–4) fragmented from a $(CO)^{4+}$ by the 1 MeV/u F^{4+} impact. Here b is measured from the oxygen nucleus.

ionization, i.e., $i \gg j$ or $i \ll j$, tends to induce the electron exchange between dissociated-ion pairs, C^{i+} and O^{j+}, after a direct ionization. This charge-rearrangement process will make the ionization cross section distribution more symmetric and narrower with respect to j variable.

In order to present the molecular effect clearly, we show in Fig. 9 the comparison of the multiple ionization cross sections for producing a $(CO)^{q+}$ ion between in the atomic picture and in the molecular picture. Here we assume that a $(CO)^{q+}$ ion is composed of the ion pairs $(C^{i+} + O^{j+})$ $(q = i + j)$. The open squares and the solid squares denote, respectively, the experimental data[13] and the CIEM results in the molecular picture for a CO target. On the other hand, the solid circles denote the CIEM results in the isolated-atom picture, which are obtained by the sum of the CIEM cross sections for producing the isolated C^{q+} and O^{q+} ions, and no other combinations between i and j are allowed. This picture corresponds to the case of the infinite internuclear distance in the molecular picture, so that there is no correlation between the final charges of a carbon ion and an oxygen ion. Figure 9 displays that the CIEM results in the molecular picture are in good agreement with the experimental data, though it yields a bit smaller values at low charges. In other words, the CIEM results in the isolated-atom picture could not provide a good agreement with the data. In particular, there are large deviations at high q values. As a conclusion, the molecular effect is significantly correlated with the simultaneous two-atom ionization process.

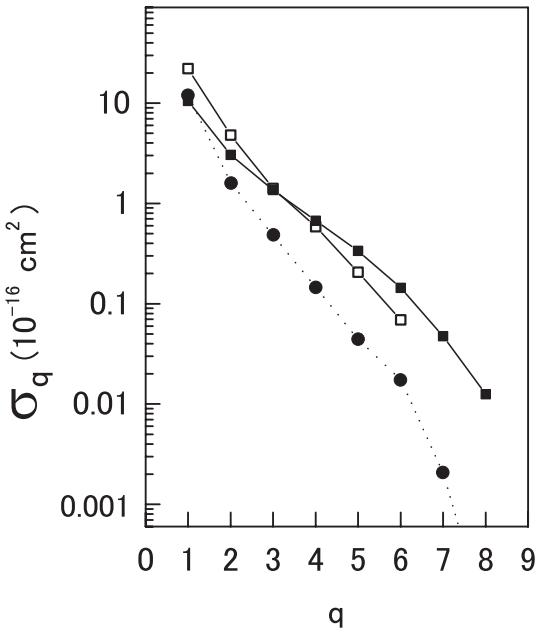

Fig. 9. σ_q for producing a $(CO)^{q+}$ ion by the 1 MeV/u F^{4+} impact. The open squares and the solid squares are the same as in Fig. 6. The solid circles denote the sum of σ_q for producing an isolated C^{q+} and that for producing an isolated O^{q+}.

In summary, we studied the multiple ionization process on the basis of the Contracted Independent Electron Model with the use of the successive ionization potential data and the modeled one-electron ionization probability. In the present picture, the molecular effect and the correlation between the molecular axis and the beam direction were well understood. In addition, any fitting parameters are not introduced. This point is a contrast to the statistical energy deposition model. Regarding the net ionization cross section of a molecule target, we proved the sum rule within this picture. It is helpful to check the validity of the calculated ionization cross sections. The sum rule implies that there is no distinction between atomic targets and molecular targets, as long as we are based on the picture that the multi-atom system is regared as the ensemble of isolated atoms. For higher charge states of fragmented ions, the study on the post-ionization rearrangement of electrons due to charge exchange among the constituent ions will be necessary for detailed comparison with the data.

Acknowledgement

One of authors (T.K.) is grateful for a partial support of a Grant-in-Aid for Scientific Research (C) from the Japan Society for the Promotion of Science (JSPS). This work is also supported by the Academic Frontier Projects by the Ministry of Education, Culture, Sports, Science and Technology (MEXT).

1) H. Knudsen, U. Mikkelsen, K. Paludan, K. Kirsebom, S. P. Møller, E. Uggerhøj, J. Slevin, M. Charlton and E. Morenzoni: J. Phys. B **28** (1995) 3569.
2) L. H. Andersen, P. Hvelplund, H. Knudsen, S. P. Møller, K. Elsener, K.-G. Rensfelt and E. Uggerhøj: Phys. Rev. Lett. **57** (1986) 2147.
3) I. Ben-Itzhak, K. D. Carnes, D. T. Johnson, P. J. Norris and O. L. Weaver: Phys. Rev. A **49** (1994) 881.
4) B. Siegmann, U. Werner, Z. Kaliman, Z. Roller-Lutz, N. M. Kabachnik and H. O. Lutz: Phys. Rev. A **66** (2002) 52701.
5) M. E. Galassi, R. D. Rivarola, M. Beuve, G. H. Olivera and P. D. Fainstein: Phys. Rev. A **62** (2000) 22701.
6) A. K. Edwards, R. M. Wood, M. A. Mangan and R. L. Ezell: Phys. Rev. A **46** (1992) 6970.
7) R. L. Ezell, A. K. Edwards, R. M. Wood, M. W. Dittmann, J. F. Browning and M. A. Mangan: Nucl. Instrum. Methods Phys. Res., Sect. B **56–57** (1991) 292.
8) S. E. Corchs, H. F. Busnengo, R. D. Rivarola and J. H. McGuire: Nucl. Instrum. Methods Phys. Res., Sect. B **117** (1996) 41.
9) N. M. Kabachnik, V. N. Kondratyev, Z. Roller-Lutz and H. O. Lutz: Phys. Rev. A **57** (1998) 990.
10) B. Siegmann, U. Werner, R. Mann, Z. Kaliman, N. M. Kabachnik and H. O. Lutz: Phys. Rev. A **65** (2001) 10704.
11) C. Caraby, A. Cassimi, L. Adoui and J. P. Grandin: Phys. Rev. A **55** (1997) 2450.

12) S. Cheng, C. L. Cocke, V. Frohne, E. Y. Kamber, J. H. McGuire and Y. Wang: Phys. Rev. A **47** (1993) 3923.
13) I. Ben-Itzhak, S. G. Ginther and K. D. Carnes: Phys. Rev. A **47** (1993) 2827.
14) I. Ben-Itzhak, S. G. Ginther and K. D. Carnes: Nucl. Instrum. Methods Phys. Res., Sect. B **66** (1992) 401.
15) V. Krishnamurthi, I. Ben-Itzhak and K. D. Carnes: J. Phys. B **29** (1996) 287.
16) G. Sampoll, R. L. Watson, O. Heber, V. Horvat, K. Wohrer and M. Chabot: Phys. Rev. A **45** (1992) 2903.
17) E. Wells, I. Ben-Itzhak, K. D. Carnes and V. Krishnamurthi: Phys. Rev. A **60** (1999) 3734.
18) P. Lablanquie, J. Delwiche, M.-J. Hubin-Franskin, I. Nenner, P. Morin, K. Ito, J. H. D. Eland, J.-M. Robbe, G. Gandara, J. Fournier and P. G. Fournier: Phys. Rev. A **40** (1989) 5673.
19) I. Ben-Itzhak, K. D. Carnes, S. G. Ginther, D. T. Johnson, P. J. Norris and O. L. Weaver: Phys. Rev. A **47** (1993) 3748.
20) A. K. Edwards and R. M. Wood: J. Chem. Phys. **76** (1982) 2938.
21) T. Tonuma, M. Kase, T. Kambara, H. Kumagai, T. Matsuo, J. Urakawa, H. Shibata, J. Takahasi, S. Özkök, S. H. Be, I. Kohno and H. Tawara: J. Phys. B **17** (1984) L317.
22) M. Saito, Y. Haruyama, N. Hamamoto, K. Yoshida, A. Itoh and N. Imanishi: J. Phys. B **28** (1995) 5117.
23) M. Saito, Y. Haruyama, K. Yoshida, A. Itoh and N. Imanishi: J. Phys. B **30** (1997) 115.
24) H. Tawara, T. Tonuma, H. Kumagai and T. Matsuo: Phys. Rev. A **41** (1990) 116.
25) T. Tonuma, H. Kumagai, T. Matsuo and H. Tawara: Phys. Rev. A **40** (1989) 6238.
26) T. H. McGuire and L. Weaver: Phys. Rev. A **16** (1977) 41.
27) I. Ben-Itzhak, T. J. Gray, J. C. Legg and J. H. McGuire: Phys. Rev. A **37** (1988) 3685.
28) T. Kirchner, L. Gulyás, R. Moshammer, M. Schulz and J. Ullrich: Phys. Rev. A **65** (2002) 42727.
29) J. M. Hansteen, O. M. Johnsen and L. Kocbach: At. Data Nucl. Data Tables **15** (1975) 305.
30) A. Russek and J. Meli: Physica **46** (1970) 222.
31) C. L. Cocke: Phys. Rev. A **20** (1979) 749.
32) N. M. Kabachnik, V. N. Kondratyev, Z. Roller-Lutz and H. O. Lutz: Phys. Rev. A **56** (1997) 2848.
33) A. Reinköster, U. Werner, N. M. Kabachnik and H. O. Lutz: Phys. Rev. A **64** (2001) 23201.
34) For example, T. Matsuo, T. Tonuma, H. Kumagai and H. Tawara: Phys. Rev. A **50** (1994) 1178.
35) T. Kaneko and T. Wada: submitted.
36) L. D. Landau and E. M. Lifshitz: *Quantum Mechanics (Non-relativistic Theory)* (Pergamon Press, 1977) 3rd ed.
37) The inter-nuclear potential $V(R)$ changes the inelatic transition amplitude $a(t)$ at time t by the factor $\exp[-\mathrm{i}/(\hbar v)\int_{t_0}^{t} V(\sqrt{b^2+z^2})\mathrm{d}z]$. Therefore, there comes no change in the transition probability $|a(t)|^2$.
38) J. D. Jackson: *Classical Electrodynamics* (John Wiley & Sons, 1975) 2nd ed., Chap. 13.
39) For example, H. Kudo: *Ion-Induced Electron Emission from Crystalline Solids* (Springer, 2002).
40) T. Kaneko: Phys. Rev. A **33** (1986) 1602.
41) E. Bonderup and P. Hvelplund: Phys. Rev. A **4** (1971) 562; T. Kaneko and Y. Yamamura: Phys. Rev. A **33** (1986) 1653.
42) S. Bashkin and J. O. Stoner, Jr.: *Atomic Energy Levels and Grotrian Diagrams* (North-Holland, 1975) Vol. 1.
43) P. E. Cade and A. C. Wahl: At. Data Nucl. Data Tables **13** (1974) 339.
44) E. S. Solov'ev, R. N. Il'in, V. A. Oparim and N. V. Fedorenko: Sov. Phys. JETP **15** (1962) 459.